

Supporting Information

Multi-electron Redox Processes at a Zr(IV) Center Facilitated by an Appended Redox-Active Cobalt-Containing Metalloligand

Jeremy P. Krogman, Bruce M. Foxman, and Christine M. Thomas*

Department of Chemistry, Brandeis University, 415 South Street, Waltham, MA 02451

CONTENTS

Figure S1. ^1H NMR spectrum of $(t\text{-BuNC})\text{Co}(i\text{Pr}_2\text{PNMes})_3\text{Zr}(\text{THF})$ (2) in C_6D_6 .	S3
Figure S2. $^{31}\text{P}\{^1\text{H}\}$ NMR spectrum of $(t\text{-BuNC})\text{Co}(i\text{Pr}_2\text{PNMes})_3\text{Zr}(\text{THF})$ (2) in C_6D_6 .	S3
Figure S3. $^{13}\text{C}\{^1\text{H}\}$ NMR spectrum of $(t\text{-BuNC})\text{Co}(i\text{Pr}_2\text{PNMes})_3\text{Zr}(\text{THF})$ (2) in C_6D_6 .	S4
Figure S4. ^1H NMR spectrum of $(t\text{-BuNC})\text{Co}(i\text{Pr}_2\text{PNMes})_3\text{Zr}\equiv\text{NMes}$ (3) in C_6D_6 .	S4
Figure S5. ^1H NMR spectrum of $(t\text{-BuNC})\text{Co}(i\text{Pr}_2\text{PNMes})_2(\mu\text{-NAd})\text{Zr}(i\text{Pr}_2\text{PNMes})$ (4) in C_6D_6 .	S5
Figure S6. ^1H NMR spectrum of $(t\text{-BuNC})\text{Co}(i\text{Pr}_2\text{PNMes})_3\text{Zr}(\text{N}_2\text{CPh}_2)$ (5) in C_6D_6 .	S5
Figure S7. ^1H NMR spectrum of $(t\text{-BuNC})\text{Co}(i\text{Pr}_2\text{PNMes})_2(\mu\text{-N}_2\text{CPh}_2)\text{Zr}(i\text{Pr}_2\text{PNMes})$ (6) in C_6D_6 .	S6
Figure S8. $^{13}\text{C}\{^1\text{H}\}$ NMR spectrum of $(t\text{-BuNC})\text{Co}(i\text{Pr}_2\text{PNMes})_2(\mu\text{-N}_2\text{CPh}_2)\text{Zr}(i\text{Pr}_2\text{PNMes})$ (6) in C_6D_6 .	S6
Figure S9. $^{31}\text{P}\{^1\text{H}\}$ NMR spectrum of $(t\text{-BuNC})\text{Co}(i\text{Pr}_2\text{PNMes})_2(\mu\text{-N}_2\text{CPh}_2)\text{Zr}(i\text{Pr}_2\text{PNMes})$ (6) in C_6D_6 .	S7
Figure S10. Variable temperature ($-60\text{ }^\circ\text{C}$ to $+60\text{ }^\circ\text{C}$) $^{31}\text{P}\{^1\text{H}\}$ NMR spectra of $(t\text{-BuNC})\text{Co}(i\text{Pr}_2\text{PNMes})_2(\mu\text{-N}_2\text{CPh}_2)\text{Zr}(i\text{Pr}_2\text{PNMes})$ (6) in toluene- d_8 .	S7

Figure S11. Aromatic region of the variable temperature (-60 °C to +60 °C) ¹ H NMR spectra of (^t BuNC)Co(ⁱ Pr ₂ PNMes) ₂ (μ-N ₂ CPh ₂)Zr(ⁱ Pr ₂ PNMes) (6) in toluene- <i>d</i> ₈ .	S8
Figure S12. Aliphatic region of the variable temperature (-60 °C to +60 °C) ¹ H NMR spectra of (^t BuNC)Co(ⁱ Pr ₂ PNMes) ₂ (μ-N ₂ CPh ₂)Zr(ⁱ Pr ₂ PNMes) (6) in toluene- <i>d</i> ₈ .	S9
Figure S13. ¹ H NMR spectrum of (^t BuNC)Co(ⁱ Pr ₂ PNMes) ₃ Zr(μ ₂ -κ ¹ -O-η ² -N,N-OC(OEt)CHN ₂)Zr(MesNP ⁱ Pr ₂) ₃ Co(CN ^t Bu) (7) in C ₆ D ₆ .	S9
Table S1. X-ray Diffraction Experimental Details for 3 , 4 , and 5 .	S10
Table S2. X-ray Diffraction Experimental Details for 6 and 7 .	S11
Figure S14. Fully labelled displacement ellipsoid representation of (^t BuNC)Co(ⁱ Pr ₂ PNMes) ₃ Zr≡NMes (3 •C ₄ H ₈ O).	S12
X-Ray data collection, solution, and refinement details for 3 •C ₄ H ₈ O.	S12-S15
Figure S15. Fully labelled displacement ellipsoid representation of (^t BuNC)Co(ⁱ Pr ₂ PNMes) ₂ (μ-NAd)Zr(ⁱ Pr ₂ PNMes) (4 •C ₄ H ₁₀ O).	S16
X-Ray data collection, solution, and refinement details for 4 •C ₄ H ₁₀ O.	S16-S17
Figure S16. Fully labelled displacement ellipsoid representation of (^t BuNC)Co(ⁱ Pr ₂ PNMes) ₃ Zr(N ₂ CPh ₂) (5).	S18
X-Ray data collection, solution, and refinement details for 5 .	S18-S19
Figure S17. Fully labelled displacement ellipsoid representation of (^t BuNC)Co(ⁱ Pr ₂ PNMes) ₂ (μ-N ₂ CPh ₂)Zr(ⁱ Pr ₂ PNMes) (6 •Et ₂ O).	S20
X-Ray data collection, solution, and refinement details for 6 •Et ₂ O.	S20-S21
Figure S18. Fully labelled displacement ellipsoid representation of (^t BuNC)Co(ⁱ Pr ₂ PNMes) ₃ Zr(μ ₂ -κ ¹ -O-η ² -N,N-OC(OEt)CHN ₂)Zr(MesNP ⁱ Pr ₂) ₃ Co(CN ^t Bu) (7 •2(C ₇ H ₈)).	S22
X-Ray data collection, solution, and refinement details for 7 •2(C ₇ H ₈).	S22-S24
References	S25

Figure S1. ^1H NMR spectrum of $(t\text{-BuNC})\text{Co}(t\text{-Pr}_2\text{PNMe})_3\text{Zr}(\text{THF})$ (**2**) in C_6D_6 . Trace residual solvents ($\text{C}_6\text{D}_5\text{H}$, Et_2O , pentane) are denoted with a *.

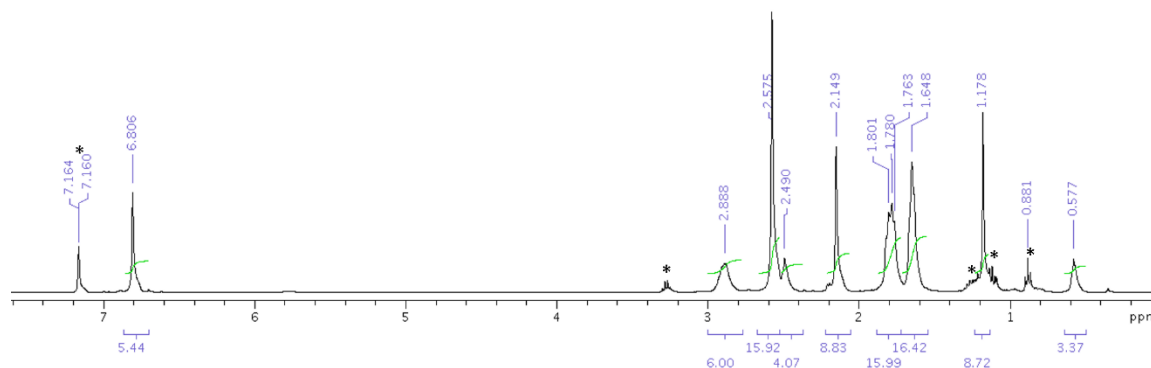


Figure S2. $^{31}\text{P}\{^1\text{H}\}$ NMR spectrum of $(t\text{-BuNC})\text{Co}(t\text{-Pr}_2\text{PNMe})_3\text{Zr}(\text{THF})$ (**2**) in C_6D_6 . Broad signal from 40-70 ppm corresponds to compound **2**. Sharper resonances with much smaller integration are also observed at 108.9 ppm and 13 ppm, although no additional diamagnetic species are observed by ^1H NMR. Isocyanide ligands have been shown to insert into early/late heterobimetallic bonds,¹ so it is hypothesized that over the long data collection time required to observe the broad ^{31}P NMR resonance, a concentrated solution of **2** undergoes a slow further reaction or decomposition process. For this reason, complex **2** was generated *in situ* for all studies of its further reactivity.

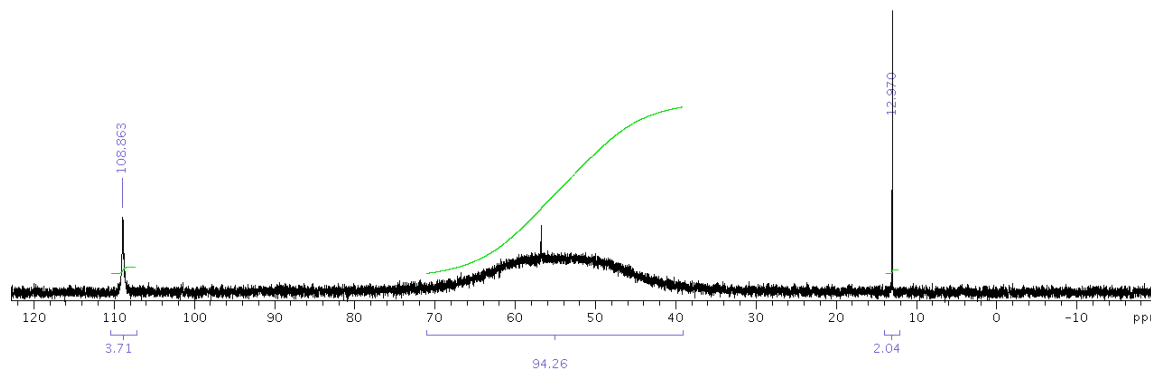


Figure S3. $^{13}\text{C}\{^1\text{H}\}$ NMR spectrum of $(t\text{BuNC})\text{Co}(i\text{Pr}_2\text{PNMe}_s)_3\text{Zr}(\text{THF})$ (**2**) in C_6D_6 . Trace residual solvents (C_6D_6 , Et_2O , pentane, THF) are denoted with a *.

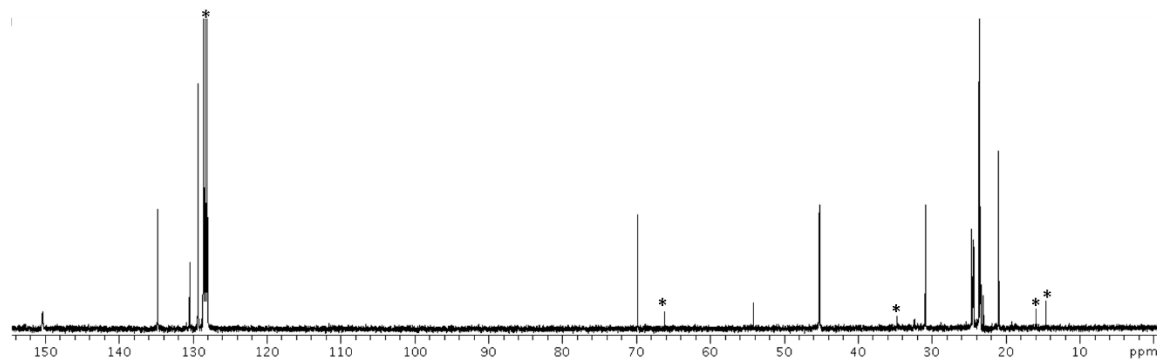


Figure S4. ^1H NMR spectrum of $(t\text{BuNC})\text{Co}(i\text{Pr}_2\text{PNMe}_s)_3\text{Zr}\equiv\text{NMes}$ (**3**) in C_6D_6 . Trace residual solvents ($\text{C}_6\text{D}_5\text{H}$ and Et_2O) are denoted with a *.

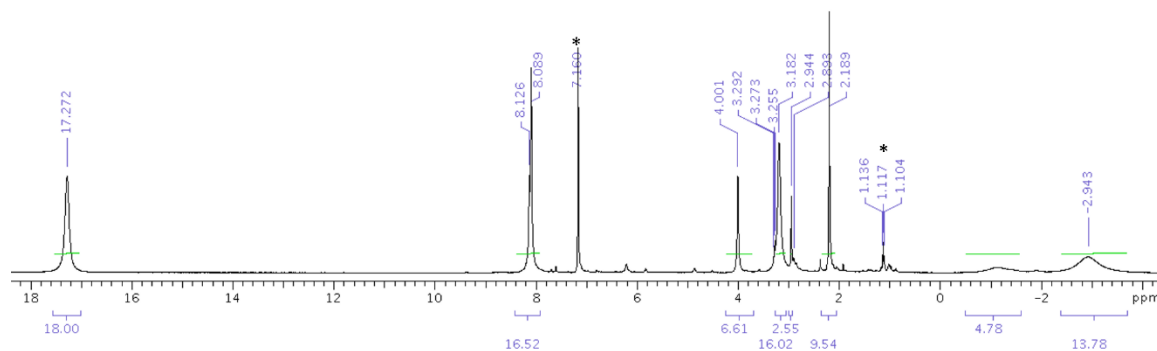


Figure S5. ^1H NMR spectrum of $(^t\text{BuNC})\text{Co}(^i\text{Pr}_2\text{PNMe}_s)_2(\mu\text{-NAd})\text{Zr}(^i\text{Pr}_2\text{PNMe}_s)$ (**4**) in C_6D_6 . Trace residual solvents ($\text{C}_6\text{D}_5\text{H}$, pentane, THF) are denoted with a *.

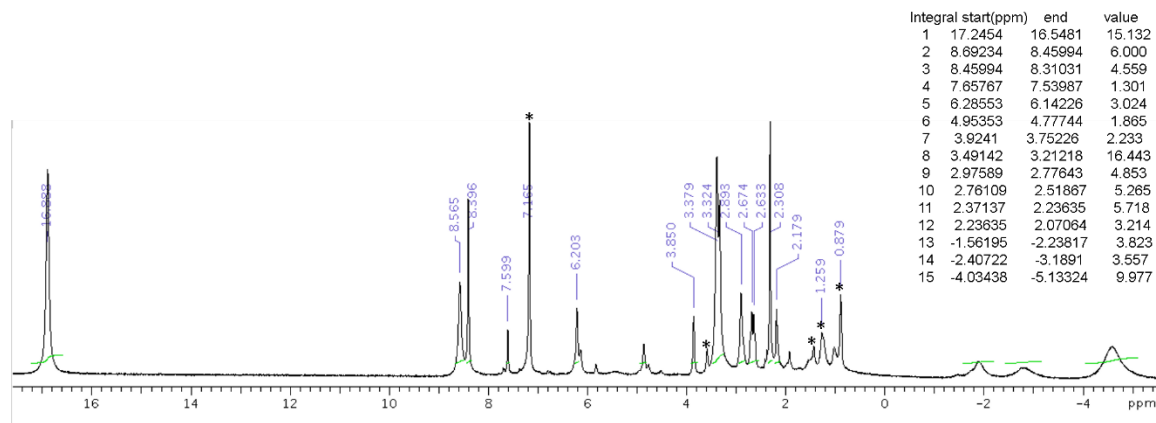


Figure S6. ^1H NMR spectrum of $(^t\text{BuNC})\text{Co}(^i\text{Pr}_2\text{PNMe}_s)_3\text{Zr}(\text{N}_2\text{CPh}_2)$ (**5**) in C_6D_6 . Trace residual solvents ($\text{C}_6\text{D}_5\text{H}$, THF, pentane, and Et_2O) are denoted with a *.

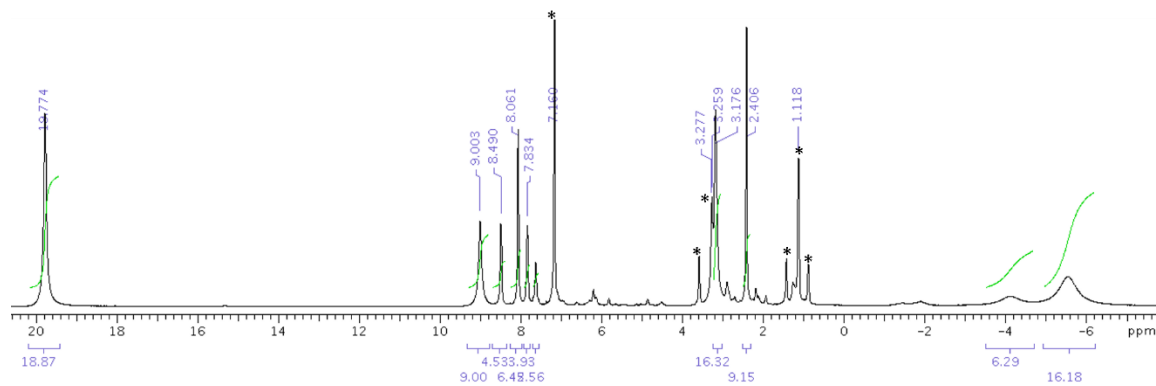


Figure S7. ^1H NMR spectrum of $(t\text{-BuNC})\text{Co}(i\text{Pr}_2\text{PNMe}_s)_2(\mu\text{-N}_2\text{CPh}_2)\text{Zr}(i\text{Pr}_2\text{PNMe}_s)$ (**6**) in C_6D_6 . Trace residual solvents ($\text{C}_6\text{D}_5\text{H}$, pentane, and $(\text{Me}_3\text{Si})_2\text{O}$) are denoted with a *.

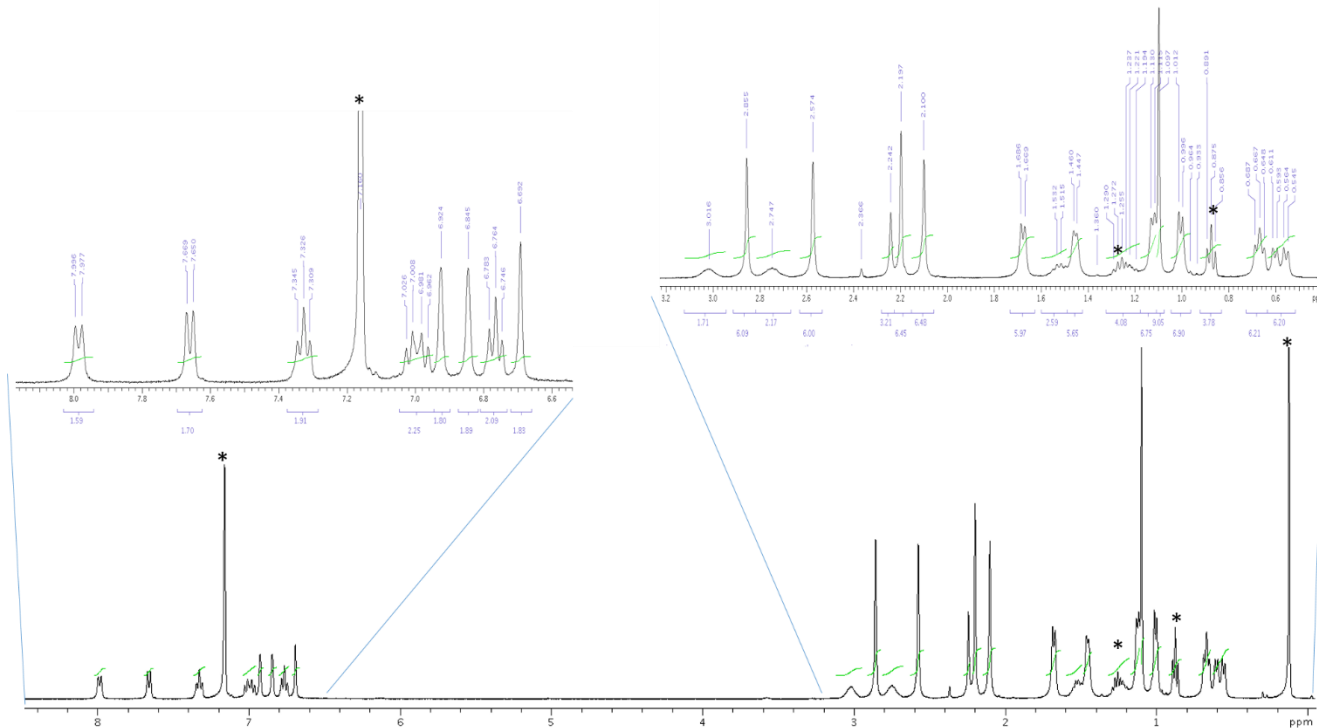


Figure S8. $^{13}\text{C}\{^1\text{H}\}$ NMR spectrum of $(t\text{-BuNC})\text{Co}(i\text{Pr}_2\text{PNMe}_s)_2(\mu\text{-N}_2\text{CPh}_2)\text{Zr}(i\text{Pr}_2\text{PNMe}_s)$ (**6**) in C_6D_6 . C_6D_6 is denoted with a *.

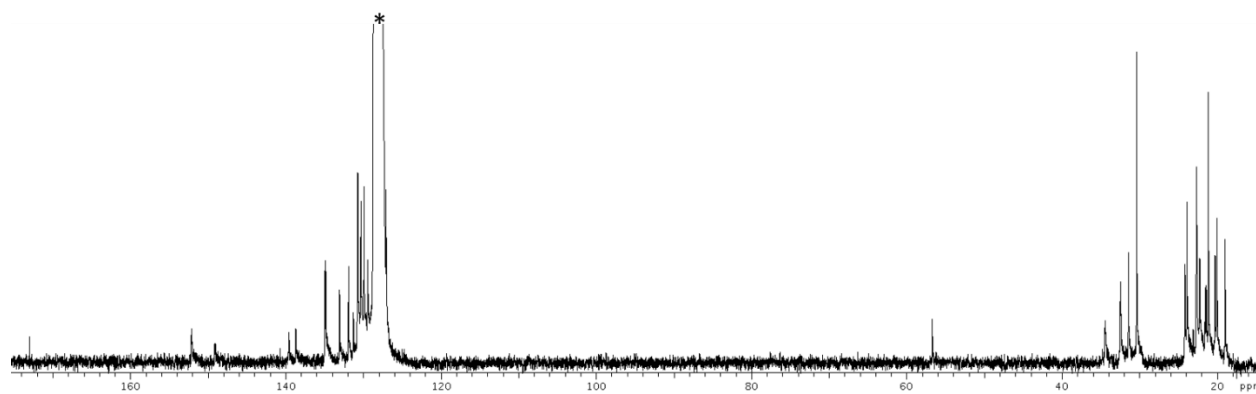


Figure S9. $^{31}\text{P}\{^1\text{H}\}$ NMR spectrum of $(^t\text{BuNC})\text{Co}(i\text{Pr}_2\text{PNMes})_2(\mu\text{-N}_2\text{CPh}_2)\text{Zr}(i\text{Pr}_2\text{PNMes})$ (**6**) in C_6D_6 at room temperature.

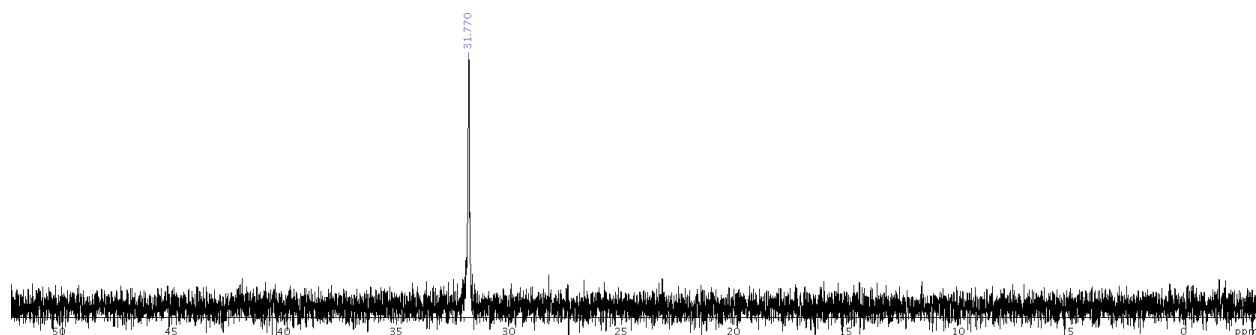


Figure S10. Variable temperature ($-60\text{ }^\circ\text{C}$ to $+60\text{ }^\circ\text{C}$) $^{31}\text{P}\{^1\text{H}\}$ NMR spectra of $(^t\text{BuNC})\text{Co}(i\text{Pr}_2\text{PNMes})_2(\mu\text{-N}_2\text{CPh}_2)\text{Zr}(i\text{Pr}_2\text{PNMes})$ (**6**) in toluene- d_8 .

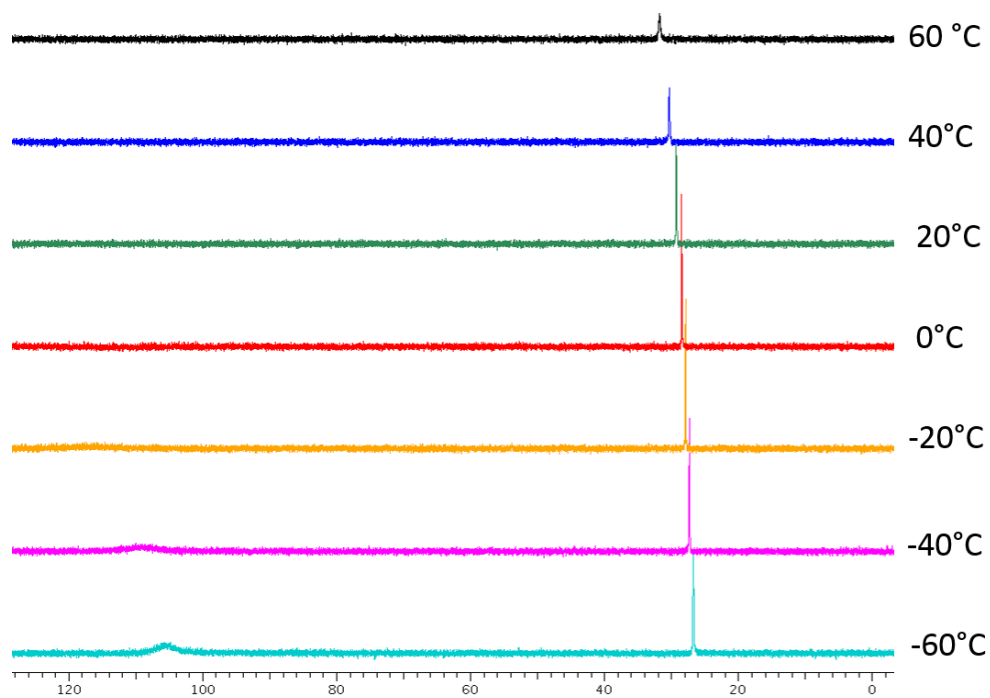


Figure S11. Aromatic region of the variable temperature (-60 °C to +60 °C) ^1H NMR spectra of $(^i\text{BuNC})\text{Co}(^i\text{Pr}_2\text{PNMe}_s)_2(\mu\text{-N}_2\text{CPh}_2)\text{Zr}(^i\text{Pr}_2\text{PNMe}_s)$ (**6**) in toluene- d_8 . Resonances for toluene- d_8 and residual C_6H_6 are denoted with a *.

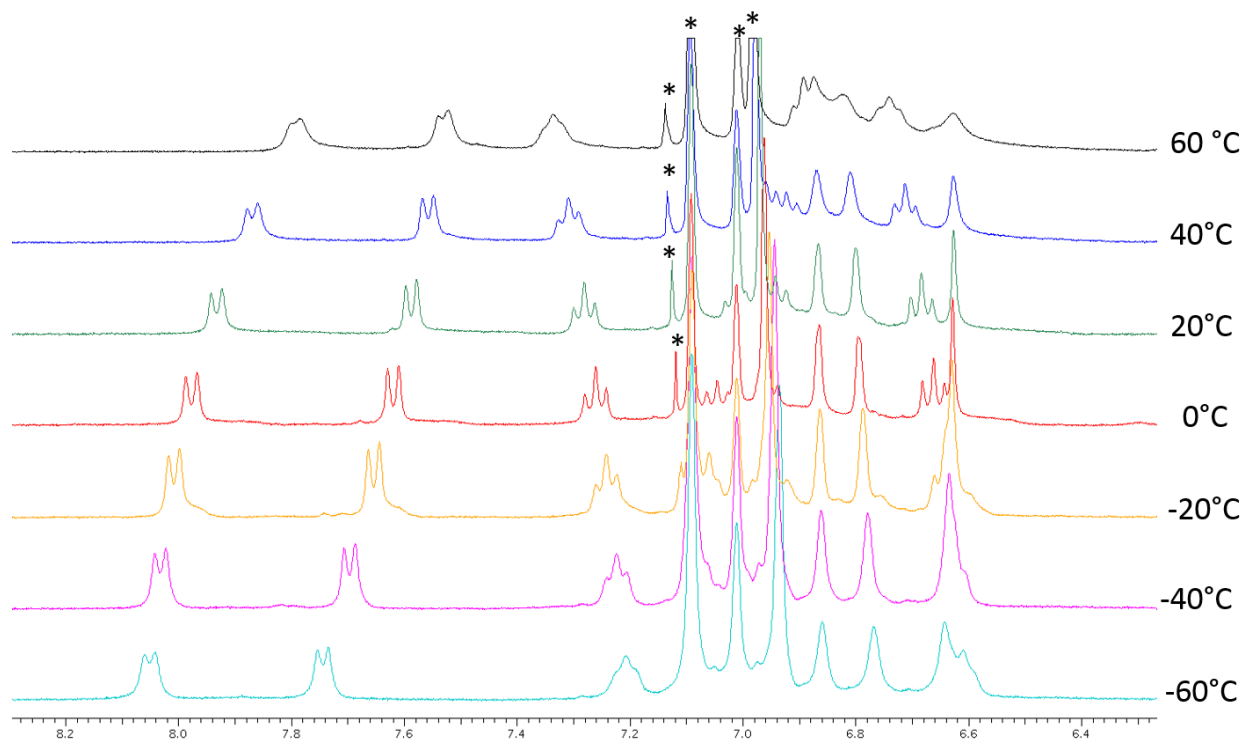


Figure S12. Aliphatic region of the variable temperature (-60 °C to +60 °C) ^1H NMR spectra of $(^i\text{BuNC})\text{Co}(^i\text{Pr}_2\text{PNMe})_2(\mu\text{-N}_2\text{CPh}_2)\text{Zr}(^i\text{Pr}_2\text{PNMe})$ (**6**) in toluene- d_8 . Resonances for toluene- d_8 and residual pentane are denoted with a *.

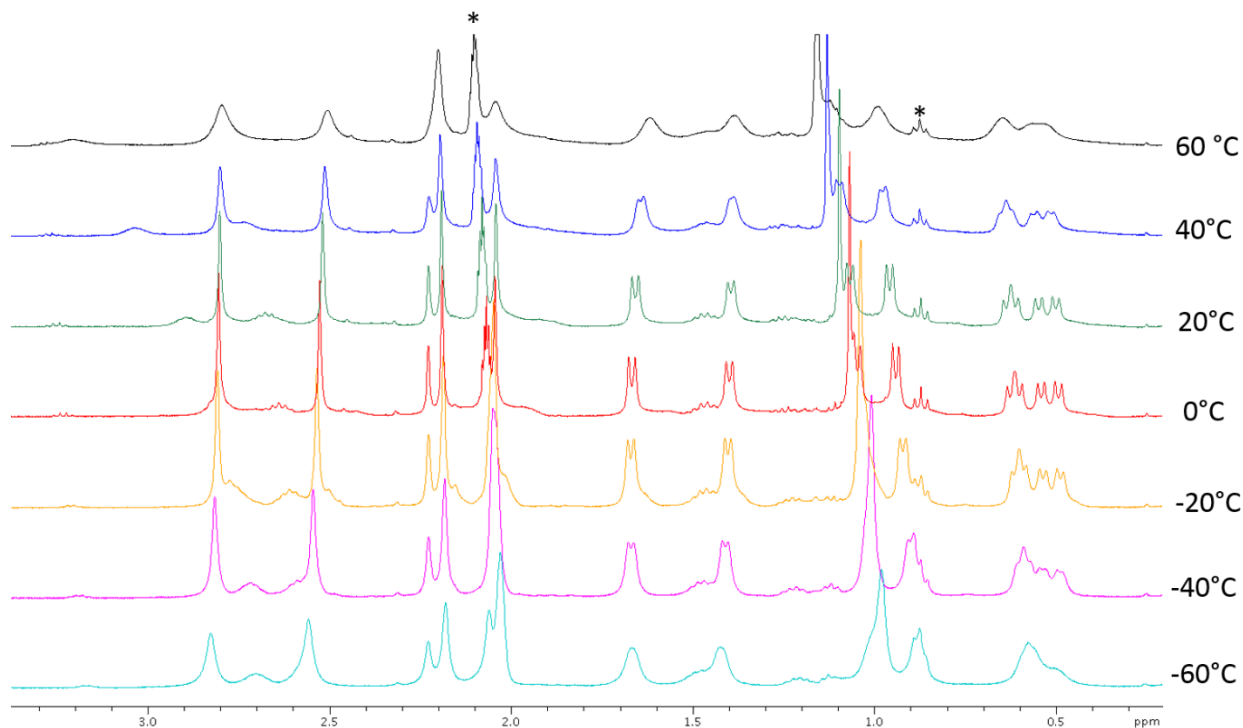


Figure S13. ^1H NMR spectrum of $(^i\text{BuNC})\text{Co}(^i\text{Pr}_2\text{PNMe})_3\text{Zr}(\mu_2\text{-}\kappa^1\text{-O-}\eta^2\text{-N,N-OC(OEt)CHN}_2)\text{Zr}(\text{MesNP}^i\text{Pr}_2)_3\text{Co}(\text{CN}^i\text{Bu})$ (**7**) in C_6D_6 . Trace residual solvents ($\text{C}_6\text{D}_5\text{H}$ and pentane) are denoted with a *.

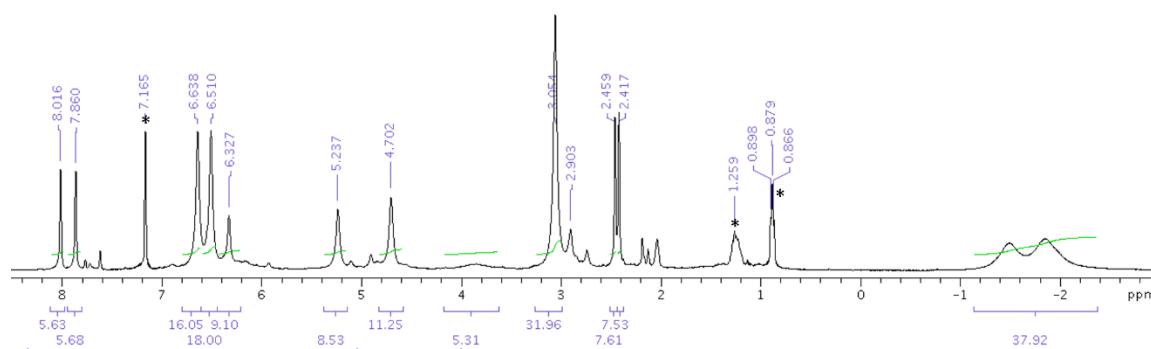


Table S1. X-ray Diffraction Experimental Details for **3**, **4**, and **5**.

	3•C₄H₈O	4•C₄H₁₀O	5
chemical formula	C ₆₃ H ₁₀₃ N ₅ OP ₃ CoZr	C ₆₄ H ₁₀₉ N ₅ OP ₃ CoZr	C ₆₃ H ₉₄ N ₆ P ₃ CoZr
fw	1189.62	1207.68	1178.55
<i>T</i> (K)	120	120	120
λ (Å)	0.71073	0.71073	0.71073
<i>a</i> (Å)	12.6423(4)	19.1053(5)	11.8670(3)
<i>b</i> (Å)	12.9539(4)	11.8605(3)	22.1741(6)
<i>c</i> (Å)	21.9518(7)	28.6132(7)	23.7819(7)
α (°)	89.6031(17)	90	90
β (°)	74.4605(15)	92.5530(10)	93.5286(14)
γ (°)	75.7836(15)	90	90
<i>V</i> (Å ³)	3350.82(11)	6477.27(16)	6246.11(18)
space group	<i>P</i> 1̄	<i>P</i> 2 ₁ / <i>c</i>	<i>P</i> 2 ₁ / <i>c</i>
<i>Z</i> , <i>Z</i> '	2, 1	4, 1	4, 1
<i>D</i> _{calc} (g/cm ³)	1.179	1.238	1.253
μ (cm ⁻¹)	5.15	5.34	5.51
R1 (<i>I</i> > 2 σ (<i>I</i>)), wR2 ^a	0.0505, 0.1307	0.0323, 0.0816	0.0300, 0.0766

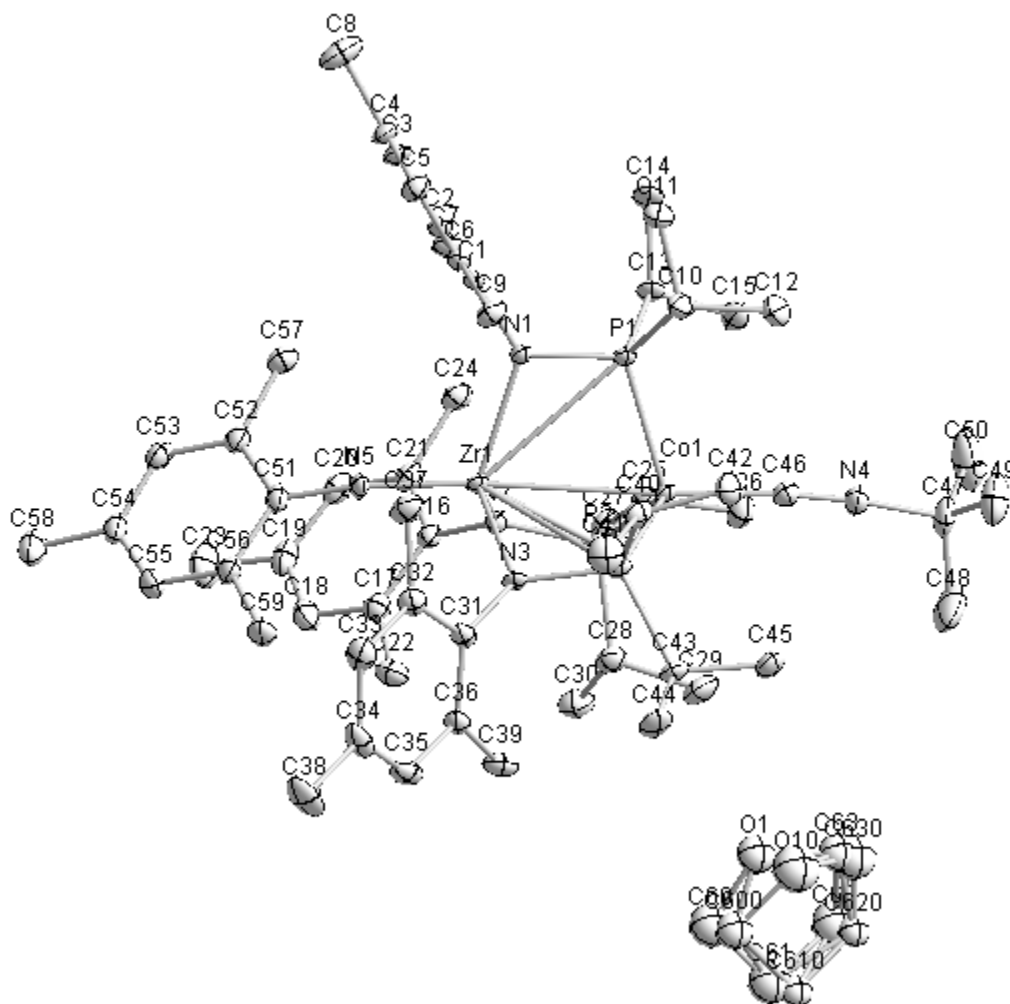
$$^a \text{R1} = \frac{\sum ||F_o| - |F_c||}{\sum |F_o|}, \text{wR2} = \left(\frac{\sum [w(F_o^2 - F_c^2)^2]}{\sum [w(F_o^2)^2]} \right)^{1/2}$$

Table S2. X-ray Diffraction Experimental Details for **6** and **7**.

	6•Et₂O	7•2(C₇H₈)
chemical formula	C ₆₇ H ₁₀₄ CoN ₆ OP ₃ Zr	C ₁₁₈ H ₁₉₀ N ₁₀ O ₂ P ₆ Co ₂ Zr ₂
fw	1252.68	2266.93
<i>T</i> (K)	120	120
λ (Å)	0.71073	0.71073
<i>a</i> (Å)	11.2422(2)	15.3717(4)
<i>b</i> (Å)	15.6852(3)	16.3072(4)
<i>c</i> (Å)	38.6830(9)	27.7262(7)
α (°)	90	87.6338(11)
β (°)	90.0071(14)	86.3298(11)
γ (°)	90	69.9841(12)
<i>V</i> (Å ³)	6821.2(2)	6515.52(16)
space group	<i>P</i> 2 ₁ / <i>n</i>	<i>P</i> 1̄
<i>Z</i> , <i>Z</i> '	4, 1	2, 1
<i>D</i> _{calc} (g/cm ³)	1.220	1.155
μ (cm ⁻¹)	5.10	5.27
R1 (<i>I</i> > 2 σ (<i>I</i>)), wR2 ^a	0.0318, 0.0809	0.0468, 0.1088

^a $R1 = \sum ||F_o| - |F_c|| / \sum |F_o|$, $wR2 = (\sum [w(F_o^2 - F_c^2)^2] / \sum [w(F_o^2)^2])^{1/2}$

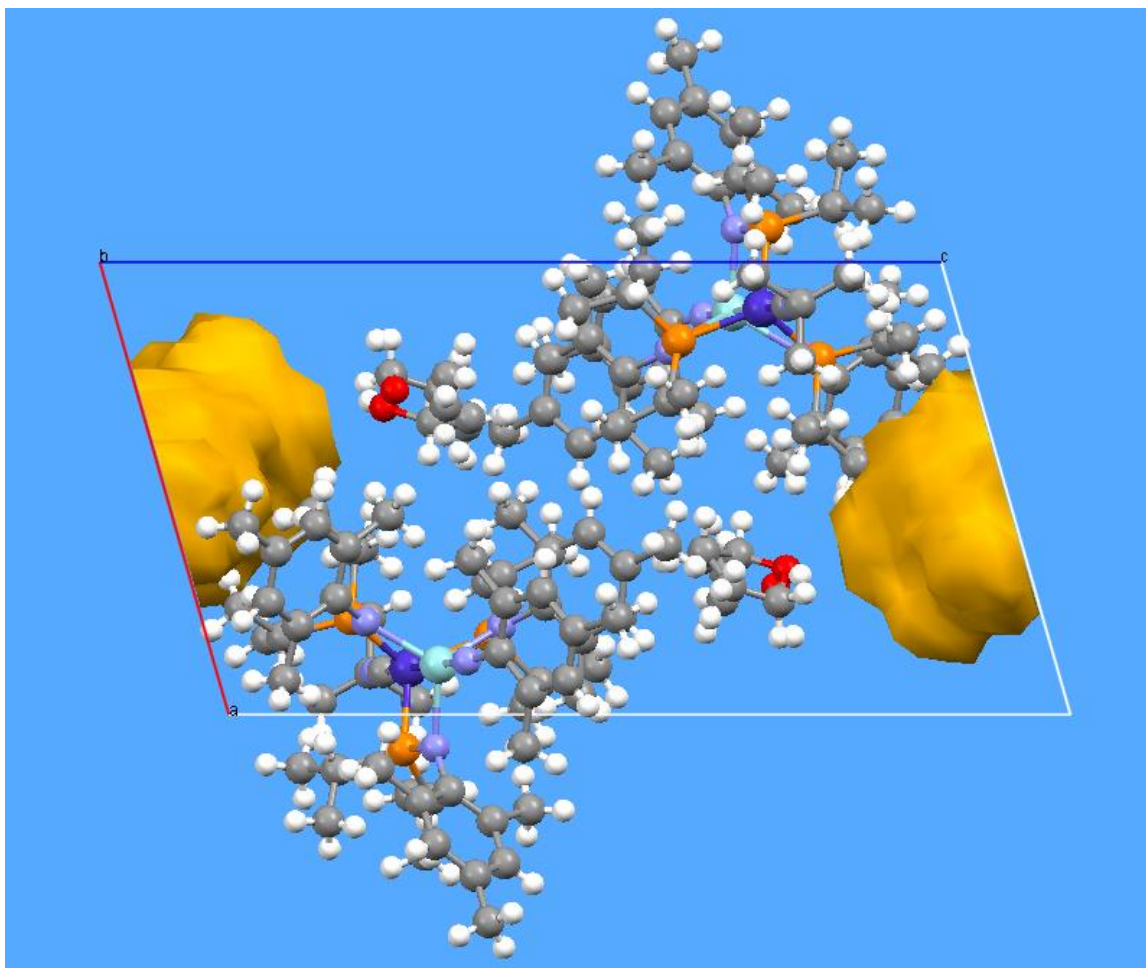
Figure S14. Fully labelled displacement ellipsoid representation of (*t*-BuNC)Co(*i*-Pr₂PNMes)₃Zr≡NMes (**3**•C₄H₈O).



X-Ray data collection, solution, and refinement details for 3•C₄H₈O. All operations were performed on a Bruker-Nonius Kappa Apex2 diffractometer, using graphite-monochromated MoK α radiation. All diffractometer manipulations, including data collection, integration, scaling, and absorption corrections were carried out using the Bruker Apex2 software.² Preliminary cell constants were obtained from three sets of 12 frames. Data collection was carried out at 120K, using a frame time of 20 sec and a detector distance of 60 mm. The optimized strategy used for data collection consisted of five phi and one omega scan sets, with 0.5° steps in phi or omega;

completeness was 98.6%. A total of 3042 frames were collected. Final cell constants were obtained from the xyz centroids of 8272 reflections after integration.

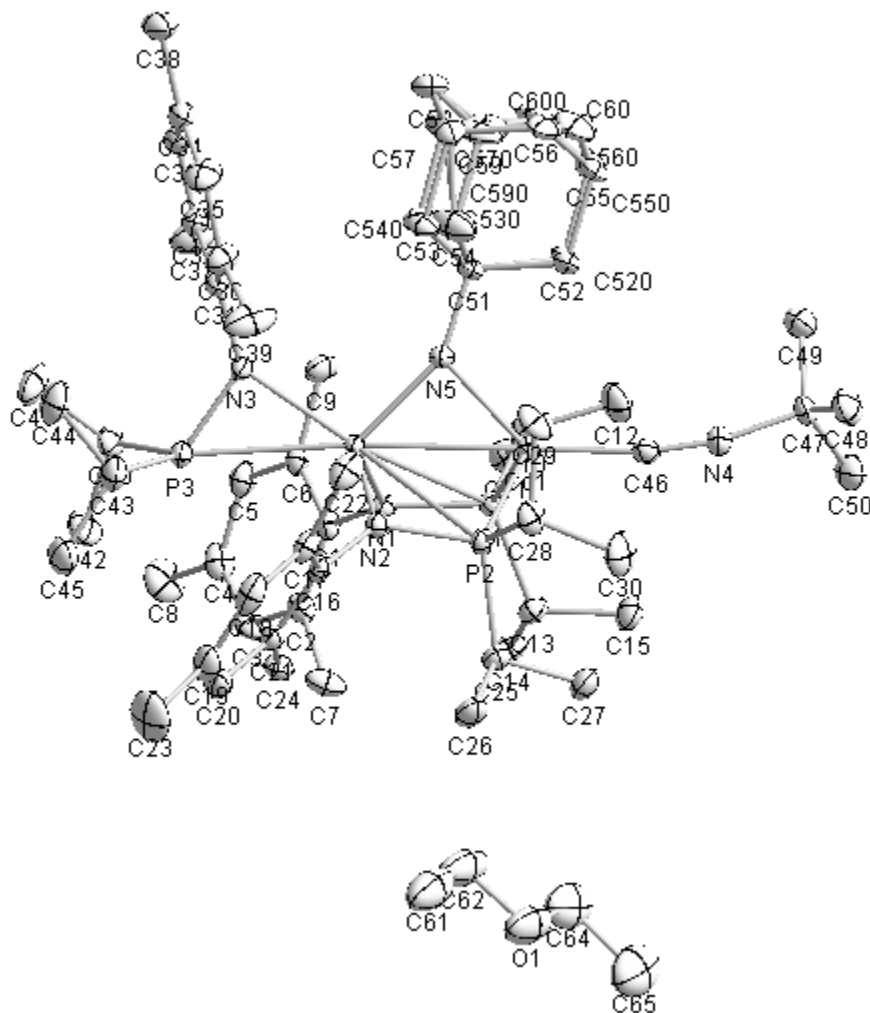
From the systematic absences, the observed metric constants and intensity statistics, space group $P\bar{1}$ was chosen initially; subsequent solution and refinement confirmed the correctness of this choice. The structure was solved using *SIR-92*,³ and refined (full-matrix-least squares) using the Oxford University *Crystals for Windows* program.⁴ The asymmetric unit contains one molecule of complex ($Z = 2$; $Z' = 1$). All ordered non-hydrogen atoms were refined using anisotropic displacement parameters. After location of H atoms on electron-density difference maps, the H atoms were initially refined with soft restraints on the bond lengths and angles to regularise their geometry (C---H in the range 0.93--0.98 Å and U_{iso} (H) in the range 1.2-1.5 times U_{eq} of the parent atom), after which the positions were refined with riding constraints.⁵ During the structure solution, electron density difference maps revealed that there were likely two molecules of solvent in the asymmetric unit. From history, the remaining solvate was likely tetrahydrofuran (THF). One of the molecules of THF was in a volume of 314 Å³ per unit cell (9.4%). It appeared that the cavity areas contained about two THF molecules, located near the center of symmetry at (0.500, 0.500, 0) as shown in the *ac* projection below.⁶



Modeling this THF molecule with or without restraints was unsuccessful, as was step by step acquisition of peaks using successive electron density difference maps. Thus, the structure factors were modified using the PLATON SQUEEZE⁷ technique. PLATON reported a total electron density of 62 e⁻ per unit cell, likely representing about two THF molecules, consistent with our earlier observations. Use of the SQUEEZE technique resulted in a decrease of ca. 3.8 % in *R*. The second molecule of THF was modeled by splitting the molecule into two parts and using the restraints. Occupancies of the major component: (O1, C59, C60, C61, C62, C63), and the minor component: (O10, C590, C600, C610, C620, C630), were refined while being constrained to a sum of 1. The major component occupancy refined to 0.703(13). The use of restraints on the O-C bond lengths was needed for the convergence during refinement; details appear in the CIF file.

The final least-squares refinement converged to $R_1 = 0.0505$ ($I > 2\sigma(I)$, 10838 data) and $wR_2 = 0.1307$ (F^2 , 14495 data, 663 parameters). The final CIF is available as supporting material.

Figure S15. Fully labelled displacement ellipsoid representation of $(t\text{BuNC})\text{Co}(i\text{Pr}_2\text{PNMe})_2(\mu\text{-NAd})\text{Zr}(i\text{Pr}_2\text{PNMe})$ ($4 \cdot \text{C}_4\text{H}_{10}\text{O}$).

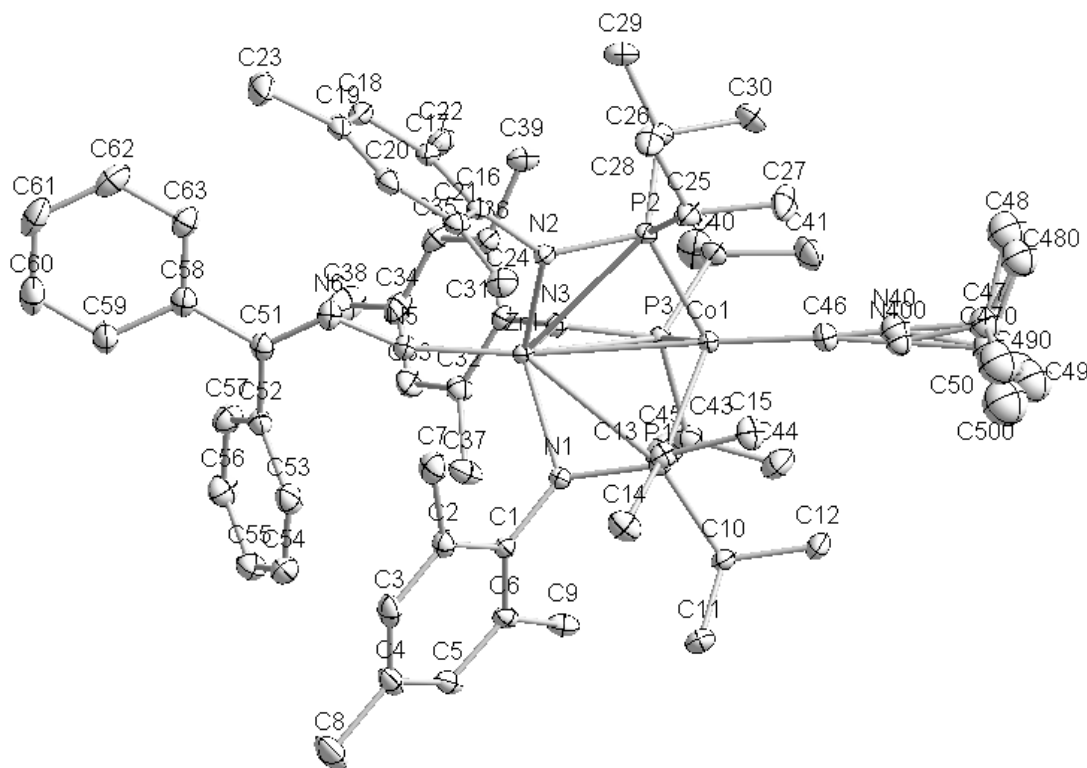


X-Ray data collection, solution, and refinement details for $4 \cdot \text{C}_4\text{H}_{10}\text{O}$. All operations were performed on a Bruker-Nonius Kappa Apex2 diffractometer, using graphite-monochromated $\text{MoK}\alpha$ radiation. All diffractometer manipulations, including data collection, integration, scaling, and absorption corrections were carried out using the Bruker Apex2 software.² Preliminary cell constants were obtained from three sets of 12 frames. Data collection was carried out at 120K, using a frame time of 20 sec and a detector distance of 60 mm. The optimized strategy used for data collection consisted of three phi and four omega scan sets, with 0.5° steps in phi or omega;

completeness was 99.6%. A total of 2116 frames were collected. Final cell constants were obtained from the xyz centroids of 9851 reflections after integration.

From the systematic absences, the observed metric constants and intensity statistics, space group $P2_1/c$ was chosen initially; subsequent solution and refinement confirmed the correctness of this choice. The structure was solved using *SIR-92*,³ and refined (full-matrix-least squares) using the Oxford University *Crystals for Windows* program.⁴ The asymmetric unit contains one molecule of complex ($Z = 4$; $Z' = 1$) and one molecule of diethyl ether. Disorder was observed in the adamantyl group of the μ -imide ligand; the disorder was successfully modeled by splitting the majority of the adamantyl group into two components. Occupancies of atoms (C(520), C(530), C(540), C(550), C(560), C(570), C(590), C(600), [minor component]) and (C(52), C(53), C(54), C(55), C(56), C(57), C(59), C(60), [major component]) were constrained to sum of 1.0; the major component occupancy refined to a value of 0.534(8). All non-hydrogen atoms were refined using anisotropic displacement parameters. After location of H atoms on electron-density difference maps, the H atoms were initially refined with soft restraints on the bond lengths and angles to regularize their geometry (C---H in the range 0.93--0.98 Å and U_{iso} (H) in the range 1.2-1.5 times U_{eq} of the parent atom), after which the positions were refined with riding constraints.⁵ The final least-squares refinement converged to $R_1 = 0.0323$ ($I > 2\sigma(I)$, 10974 data) and $wR_2 = 0.0816$ (F^2 , 14177 data, 749 parameters). The final CIF is available as supporting material.

Figure S16. Fully labelled displacement ellipsoid representation of (*t*-BuNC)Co(*i*-Pr₂PNMes)₃Zr(N₂CPh₂) (**5**).

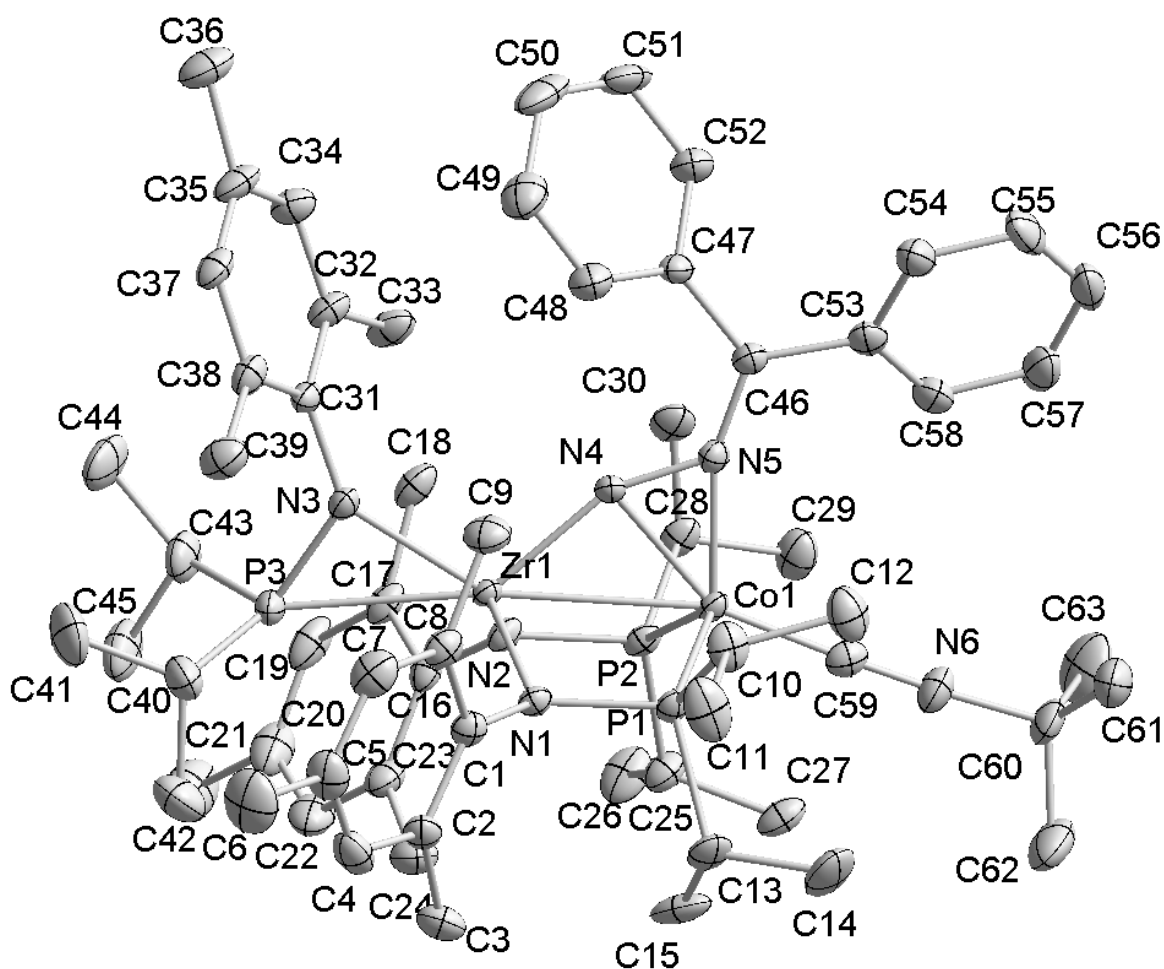


X-Ray data collection, solution, and refinement details for 5. All operations were performed on a Bruker-Nonius Kappa Apex2 diffractometer, using graphite-monochromated MoK α radiation. All diffractometer manipulations, including data collection, integration, scaling, and absorption corrections were carried out using the Bruker Apex2 software.² Preliminary cell constants were obtained from three sets of 12 frames. Data collection was carried out at 120K, using a frame time of 20 sec and a detector distance of 60 mm. The optimized strategy used for data collection consisted of three phi and one omega scan sets, with 0.5° steps in phi or omega; completeness was 99.9%. A total of 2149 frames were collected. Final cell constants were obtained from the xyz centroids of 9995 reflections after integration.

From the systematic absences, the observed metric constants and intensity statistics, space group *P*2₁/*c* was chosen initially; subsequent solution and refinement confirmed the correctness of this

choice. The structure was solved using *SIR-92*,³ and refined (full-matrix-least squares) using the Oxford University *Crystals for Windows* program.⁴ The asymmetric unit contains one molecule of complex ($Z = 4$; $Z' = 1$). All ordered non-hydrogen atoms were refined using anisotropic displacement parameters. After location of H atoms on electron-density difference maps, the H atoms were initially refined with soft restraints on the bond lengths and angles to regularize their geometry (C---H in the range 0.93--0.98 Å and U_{iso} (H) in the range 1.2-1.5 times U_{eq} of the parent atom), after which the positions were refined with riding constraints.⁵ Disorder of the Co *tert*-butyl isocyanide ligand was observed. The disorder was modeled by using two components. Occupancies of the major/minor components ((N(40);C(47);C(48);C(49);C(50))/(N(400);C(470);C(480);C(490);C(500))) were constrained to sum to 1.0; the major component occupancy for the model refined to a value of 0.587(11). Atoms from both components were refined using isotropic displacement parameters. The final least-squares refinement converged to $R_1 = 0.0300$ ($I > 2\sigma(I)$, 12150 data) and $wR_2 = 0.0766$ (F^2 , 15107 data, 663 parameters). The final CIF is available as supporting material.

Figure S17. Fully labelled displacement ellipsoid representation of (*t*-BuNC)Co(*i*-Pr₂PNMes)₂(μ-N₂CPh₂)Zr(*i*-Pr₂PNMes) (**6•Et₂O**).

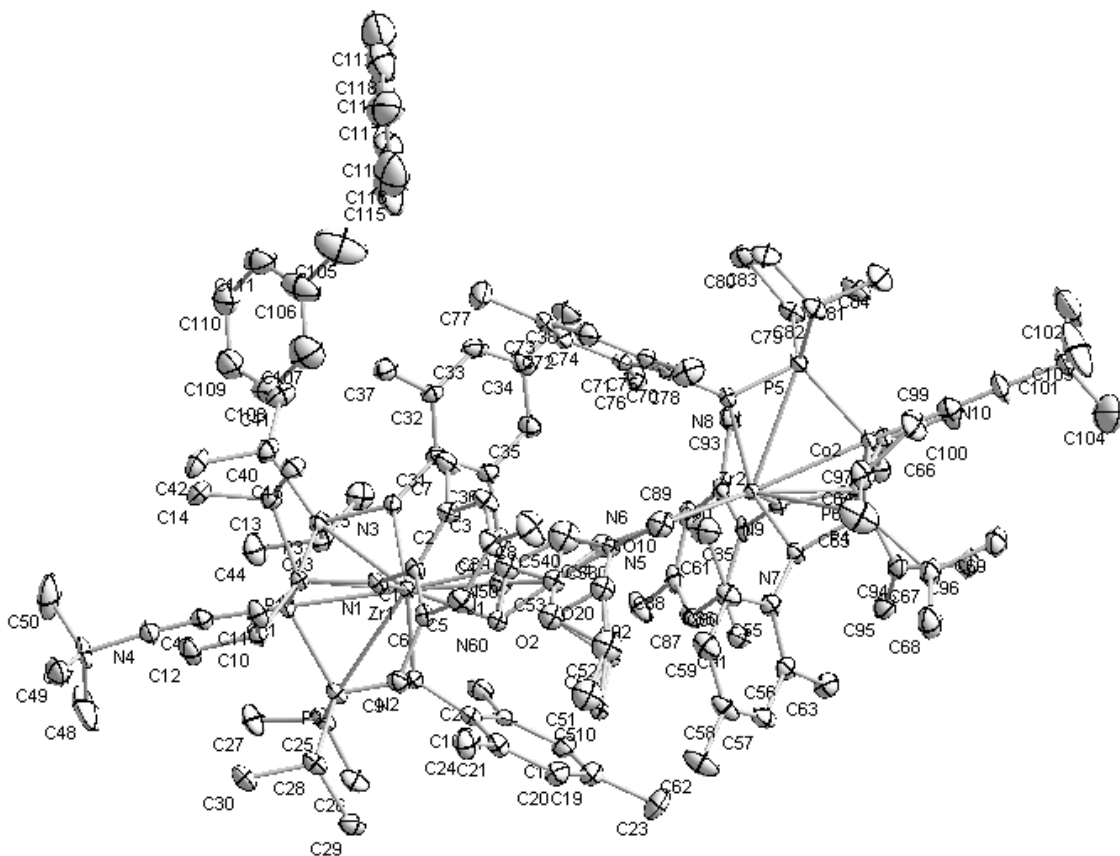


X-Ray data collection, solution, and refinement details for (6•Et₂O**).** All operations were performed on a Bruker-Nonius Kappa Apex2 diffractometer, using graphite-monochromated MoK α radiation. All diffractometer manipulations, including data collection, integration, scaling, and absorption corrections were carried out using the Bruker Apex2 software.² Preliminary cell constants were obtained from three sets of 12 frames. Data collection was carried out at 120K, using a frame time of 40 sec and a detector distance of 60 mm. The optimized strategy used for data collection consisted of five phi and two omega scan sets, with 0.5° steps in phi or omega;

completeness was 99.9%. A total of 2792 frames were collected. Final cell constants were obtained from the xyz centroids of 9832 reflections after integration.

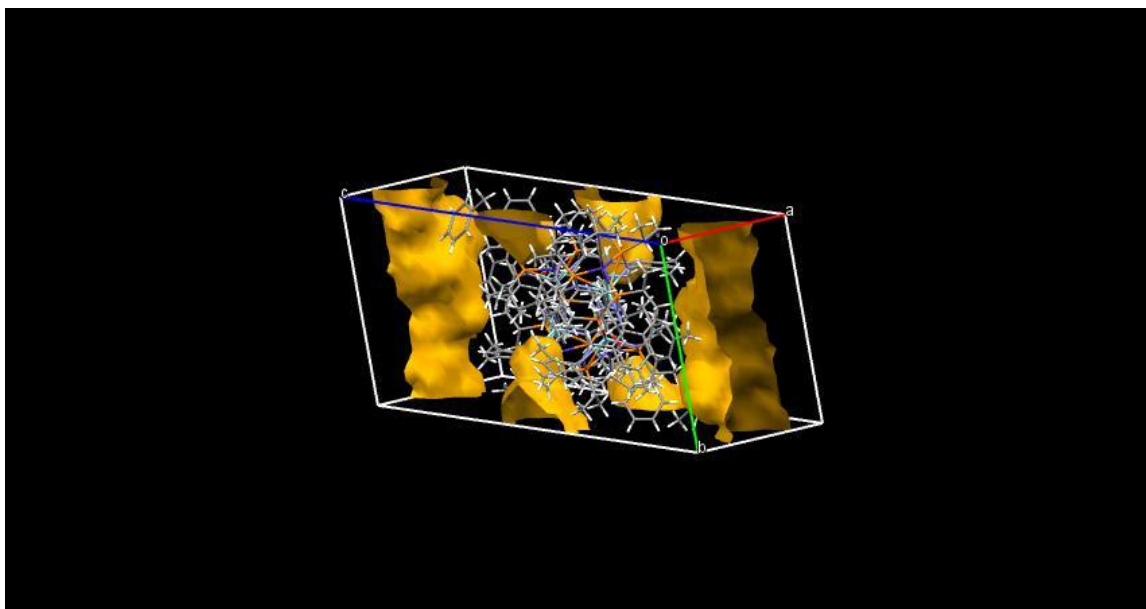
From the systematic absences, the observed metric constants and intensity statistics, space group $P2_1/n$ was chosen initially; subsequent solution and refinement confirmed the correctness of this choice. The structure was solved using *SIR-92*,³ and refined (full-matrix-least squares) using the Oxford University *Crystals for Windows* program.⁴ The asymmetric unit contains one molecule of the complex and one ether molecule ($Z = 4$; $Z' = 1$). All ordered non-hydrogen atoms were refined using anisotropic displacement parameters. After location of H atoms on electron-density difference maps, the H atoms were initially refined with soft restraints on the bond lengths and angles to regularize their geometry (C---H in the range 0.93--0.98 Å and U_{iso} (H) in the range 1.2-1.5 times U_{eq} of the parent atom), after which the positions were refined with riding constraints.⁵ Use of the ROTAX procedure in the *Crystals for Windows* software⁸ suggested a TLS Class II (i.e., pseudo-merohedral) monoclinic twin,⁹ with a rotation about the a axis, an obliquity of 0.007° and twin law (1 0 0 / 0 -1 0 / 0 0 -1). The twin component scale factors were refined, and the sum of the components was constrained to sum to 1.0, with a final value of the major component of 0.5006(5). The final least-squares refinement converged to $R_1 = 0.0318$ ($I > 2\sigma(I)$, 10734 data) and $wR_2 = 0.0809$ (F^2 , 13414 data, 713 parameters). The final CIF is available as supporting material.

Figure S18. Fully labelled displacement ellipsoid representation of $(^i\text{BuNC})\text{Co}(^i\text{Pr}_2\text{PNMes})_3\text{Zr}(\mu_2\text{-}\kappa^1\text{-O-}\eta^2\text{-N,N-OC(OEt)CHN}_2)\text{Zr}(\text{MesNP}^i\text{Pr}_2)_3\text{Co}(\text{CN}^i\text{Bu})$ (**7**•**2**(**C**₇**H**₈)).



X-Ray data collection, solution, and refinement details for 7•2(C₇H₈). All operations were performed on a Bruker-Nonius Kappa Apex2 diffractometer, using graphite-monochromated MoK α radiation. All diffractometer manipulations, including data collection, integration, scaling, and absorption corrections were carried out using the Bruker Apex2 software.² Preliminary cell constants were obtained from three sets of 12 frames. Data collection was carried out at 120K, using a frame time of 40 sec and a detector distance of 60 mm. The optimized strategy used for data collection consisted of three phi and two omega scan sets, with 0.5° steps in phi or omega; completeness was 99.8%. A total of 2470 frames were collected. Final cell constants were obtained from the xyz centroids of 9983 reflections after integration.

From the systematic absences, the observed metric constants and intensity statistics, space group $P\bar{1}$ was chosen initially; subsequent solution and refinement confirmed the correctness of this choice. The structure was solved using *SIR-92*,³ and refined (full-matrix-least squares) using the Oxford University *Crystals for Windows* program.⁴ The asymmetric unit contains one molecule of the complex two ordered toluene solvate molecules, and 1.5-2 highly disordered toluene solvate molecules (for the complex, $Z = 2$; $Z' = 1$). All ordered non-hydrogen atoms were refined using anisotropic displacement parameters. After location of H atoms on electron-density difference maps, the H atoms were initially refined with soft restraints on the bond lengths and angles to regularise their geometry (C---H in the range 0.93--0.98 Å and U_{iso} (H) in the range 1.2-1.5 times U_{eq} of the parent atom), after which the positions were refined with riding constraints.⁵ During the structure solution, only two toluene solvate molecules could be located and successfully refined or modeled; electron density difference maps revealed that there was considerable disorder involving at least three additional toluene molecules per unit cell. From history, the remaining solvate was confirmed as toluene in a volume of 837.3 Å³ per unit cell (12.9%). It appeared that the cavity areas contained approximately three (but perhaps more) toluene, located near the center of symmetry at (0, 0, .5) and in a long channel centered at the general position (0.5, 0.651, 0) as shown in the projection below.⁶



Modeling with or without restraints was unsuccessful, as was step by step acquisition of peaks using successive electron density difference maps. Thus, the structure factors were modified using the PLATON SQUEEZE⁷ technique, in order to produce a new structure factor set. PLATON reported a total electron density of 178 e⁻ per unit cell, likely representing 3-4 toluene molecules, consistent with our earlier observations. Use of the SQUEEZE technique resulted in a decrease of ca. 3.0 % in *R*. Electron-density difference maps also suggested that the bridging ethyldiazoacetate moiety was disordered. Accordingly, the two orientations were established, and refined by using isotropic displacement parameters. The occupancies of the major component and minor component were constrained to sum to 1.0; refinement led to a final occupancy of 0.848(5) for the occupancy of the minor component. Distance, angle and vibration restraints were applied to portions of the ethyldiazoacetate moiety; details may be found in the CIF file. The final least-squares refinement converged to $R_1 = 0.0468$ ($I > 2\sigma(I)$, 15320 data) and $wR_2 = 0.1088$ (F^2 , 20534 data, 1254 parameters). The final CIF file, including validation reply form items for B alerts, is available as supporting material.

References

- 1 L. H. Gade, S. Friedrich, D. J. M. Trösch, I. J. Scowen and M. McPartlin, *Inorg. Chem.*, 1999, **38**, 5295-5307.
- 2 *Apex 2, Version 2 User Manual, M86-E01078*.
- 3 A. Altomare, G. Cascarano, G. Giacovazzo, A. Guagliardi, M. C. Burla, G. Polidori and M. Camalli, *J. Appl. Cryst.*, 1994, **27**, 435-436.
- 4 (a) P. W. Betteridge, J. R. Carruthers, R. I. Cooper, K. Prout and D. J. Watkin, *J. Appl. Crystallogr.*, 2003, **36**, 1487; (b) C. K. Prout and L. J. Pearce, Cambridge Crystallography Laboratory, Oxford, UK, Editon edn., 1996.
- 5 R. I. Cooper, A. L. Thompson and D. J. Watkin, *J. Appl. Crystallogr.*, 2010, **43**, 1100-1107.
- 6 C. F. Macrae, I. J. Bruno, J. A. Chisholm, P. R. Edgington, P. McCabe, E. Pidcock, L. Rodriguez-Monge, R. Taylor, J. van de Streek and P. A. Wood, *J. Appl. Crystallogr.*, 2008, **41**, 466-470.
- 7 (a) A. L. Spek, *Acta Crystallogr., Sect. A*, 1990, **A46**, C34; (b) A. L. Spek, Utrecht University, Utrecht, The Netherlands, Editon edn., 1998; (c) P. van der Sluis and A. L. Spek, *Acta Crystallogr., Sect. A.*, 1990, **A46**, 194-201.
- 8 R. I. Cooper, R. O. Gould, S. Parsons and D. J. Watkin, *J. Appl. Crystallogr.*, 2002, **35**, 168-174.
- 9 G. Donnay and J. D. H. Donnay, *The Canadian Mineralogist*, 1974, **12**, 422-425.